MODELING AND VIBRATION CHARACTERISTICS OF A DMF BASED ON EQUIVALENT LINEARIZATION METHOD

Langwu WU[1], Liping ZENG[2*], Zihao WAN[3], Jieliang LIU[4]

To analyze the vibration characteristics of a dual mass flywheel (DMF) under the influence of variable stiffness and frictional contact in the structure, the mechanical analysis of the contact among friction block, pressure plate, and secondary flywheel in the DMF was carried out through discretization. The internal forces and torques relationship of the friction block, the pressure plate, and the secondary flywheel under the contact actions were deduced. The dynamic analysis model of the DMF and the corresponding nonlinear torsional vibration differential equation were established. The nonlinear vibration frequency characteristics, equivalent stiffness, and equivalent damping of the DMF at different input torque amplitudes were analyzed by applying equivalent linearization method. By comparing the results of numerical method and equivalent linearization method, the effectiveness of the theoretical model is verified. The results show that when the first and second stage stiffness of the DMF act simultaneously, the system response has obvious nonlinear frequency characteristics. The amplitude-frequency characteristic curve turns to right, and the frequency response curve will jump. With the increase of excitation frequency, the equivalent stiffness of the DMF increases gradually, while the equivalent damping decreases gradually.

Keywords: dual mass flywheel, discretization, nonlinear vibration, equivalent linearization

1. Introduction

To reduce the torsional vibration in automobile transmission systems, the German company LuK first proposed Dual Mass Flywheel (DMF) in the 1980s. After continuous development and refinement, the vibration reduction performance of DMF has greatly improved. More and more vehicles powered by fuel engines are now equipped with DMF [1]. DMF can reduce the first-order natural frequency of the automobile transmission system, which makes the system can run at a lower idle speed [2–4]. And DMF can also effectively alleviate the

[1] Nanchang University College of Science Technology, Gongqingcheng, 332020, China, e-mail: john119110@163.com.
[2] School of Mechatronics and Vehicle Engineering, East China Jiaotong University, Nanchang, 330013, China, e-mail: melpzeng@163.com. *Corresponding Author.
[3] School of Mechatronics and Vehicle Engineering, East China Jiaotong University, Nanchang, 330013, China, e-mail: w18720088204@163.com.
[4] School of Mechatronics and Vehicle Engineering, East China Jiaotong University, Nanchang, 330013, China, e-mail: ljl1983676142@163.com.

impact between the transmission components of vehicle powertrain, such as gear pairs, and improve the structural fatigue strength. Many researchers have conducted studies on DMF. Tang et al. [5] analyzed the influence of DMF on the torsional vibration characteristics of hybrid power trains. Berbyuk [6] optimized the DMF for the transmission system of heavy trucks. To make a DMF with piecewise variable stiffness has continuous variable stiffness, Song et al. [7] improved the structure by introducing a torque compensation device. Chen et al. [8,9] studied the nonlinear vibration characteristics of DMF with variable stiffness.

According to the principle of equivalent damping of frictions bettween relatively moving objects attenuate vibration, a friction block was introduced into a DMF in Ref [10]. There will be friction and contact between the added friction block structure, the pressure plate, and the secondary flywheel. The vibration of a mechanical system with friction and contact usually has complex nonlinear characteristics [11]. And friction and contact effects have a certain influences on vibration [12, 14]. Until now, there are few reports on the detailed modeling methods and analysis considering the friction and contact of the friction block in DMF. In addition, to meet the requirements of vibration reduction, DMF usually has multi-stage equivalent stiffness. That is, the stiffness of DMF will change at different relative angles, which also has nonlinearity. Wang et al. [15] studied the dynamic parameter matching of a multi-stage torsional stiffness DMF based on torsional vibration control by using a numerical analysis method, given the design method, and verified it through vehicle tests. Shi et al. [16] proposed an innovative arrangement of vibration absorber elements for a DMF to have multi-stage step stiffness. For matching with a vehicle under starting conditions, He et al. [17] studied the influence of a five-stages variable stiffness DMF dynamic parameters on the torsional vibration of the transmission system during engine starting. In current literatures, the influence of the friction block on vibration reduction characteristics of DMF was not thoroughly analyzed. In this work, with the consideration of the friction and contact between the friction block, the pressure plate, and the secondary flywheel, the mechanical analysis of the contact process is carried out through discretization. Then the dynamic analysis model of segmented variable stiffness DMF is established. And the nonlinear vibration frequency characteristics of DMF are analyzed by equivalent linearization method.

2. Structure of the DMF

The structure of the circumferential short spring DMF studied in this work is shown in Fig.1. One spring is installed between two spring seats, and several these assembled parts are placed in the inner cavity of the primary flywheel. The

primary flywheel in the DMF structure rotates under the action of a starting motor or engine. For shape constraints between the primary flywheel, spring seat, and secondary flywheel, power and rotating motion passed through springs are transferred to secondary flywheel and the driving part behind. In addition, the pressure plate, which wedges with friction blocks, is connected with the primary flywheel by bolts and in contact with the secondary flywheel through the axial preload to generate friction torque.

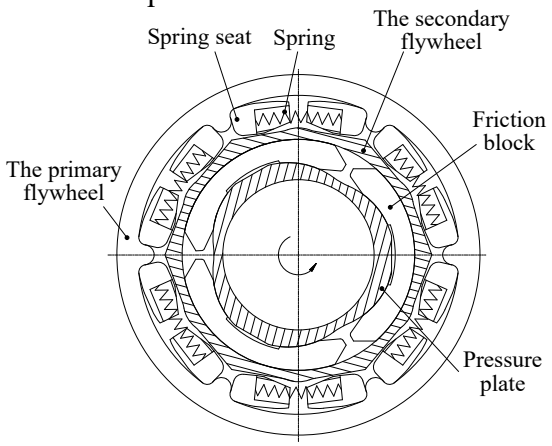

Fig.1. Structural diagram of the DMF

3. Contact analysis of the pressure plate, friction block, and secondary flywheel

The classical Hertz contact theory plays imporant role in solving elastic contact problems in practical engineering, especially for point contact [18]. But it is not suitable for the elastic deformation of point contact and finite long line contact. For problems similar to the limited length contact of friction block in this paper, the Palmgren formula is often used [19]. Assuming that the elastic modulus of the two contacting objects are E_1 and E_2, and the Poisson's ratio is υ_1 and υ_2, respectively. According to the Palmgren formula, the elastic approaching quantity δ at the contact point is:

$$\delta = 1.36 \frac{F^{0.9}}{E^{*0.9} h^{0.8}} \tag{1}$$

where, $\frac{1}{E^*} = \frac{1-\upsilon_1^2}{E_1} + \frac{1-\upsilon_2^2}{E_2}$, F is the normal load, and h is the contact thickness in the axial direction.

Compared with the pressure plate and the secondary flywheel (steel), the elastic modulus of the friction block (Pa66) is much smaller. Thus only the deformation of the friction block is considered here. As shown in Fig. 2, the contact shape between the pressure plate 3 and the friction block 2, friction block

2, and the secondary flywheel 1 are arc curves. A rectangular coordinate system *Oxy* is established. The contact curve between the pressure plate and friction block is an arc with O_1 as the center, and the eccentric distance $l_{OO1}=r_b$. The profile of the contact surface between the friction block and the secondary flywheel is an arc centered on point O. The deformation when the two parts interact is ignored. Assuming A is a contact point on the contact region between the pressure plate and the friction block when the DMF is working. The rotational angle of the pressure plate relative to the friction block is α under the action of torque. The interaction line between the pressure plate and the friction block, i.e., the arc with O_1 as the center (dotted line η_1), moves to the arc centered on O_2 (solid line η_2). At this time, the elastic deformation of the friction block at point A is $\delta_i=l_{AB}$.

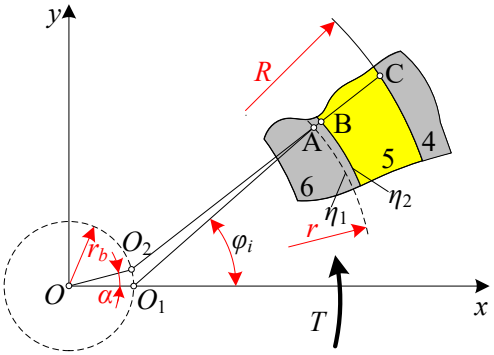

Fig. 2. Contact deformation of the friction block

The equations for the contact lines η_1 and η_2 are:

$$\begin{cases} \eta_1 : x^2 + (y - r_b)^2 = r^2 \\ \eta_2 : (x - r_b \sin\alpha)^2 + (y - r_b \cos\alpha)^2 = r^2 \end{cases} \tag{2}$$

The coordinates of contact point A before deformation are: ($r\sin\varphi_i$, $r\cos\varphi_i$). And the equation of line O_1A is: $y=x\cot\varphi_i+r_b$. The deformation of the friction block at point A in the normal direction can be obtained:

$$l_{AB} = \sqrt{r^2 - r_b^2 \left(\sin(\varphi_i - \alpha) - \sin\varphi_i\right)^2} + r_b\left(\cos(\varphi_i - \alpha) - \cos\varphi_i\right) - r \tag{3}$$

For approximate calculation, after the first three terms of the Taylor series of Equation (3) at $\alpha=0$ are conducted, the following expression can be obtained:

$$l_{AB} \approx \alpha r_b \sin\varphi_i - \frac{\alpha^2}{2} r_b \left(\cos\varphi_i + \frac{r_b}{r}\right) \approx \alpha r_b \sin\varphi_i \tag{4}$$

The force at point A can be calculated by substituting Equation (4) into Equation (1).

4. Dynamic model of the DMF

During the DMF working, the pressure plate and the primary flywheel rotate together. And the secondary flywheel and the primary flywheel interact through the spring seat-spring-spring seat structure arranged on the inner cavity of the primary flywheel (as shown in Fig. 1). For the interaction between the pressure plate and the friction block, the force on the contact surface of the pressure plate and the friction block is discretized into n component forces F_i (i=1, 2,..., n). It is assumed that the equivalent moment of inertia of the primary flywheel and the pressure plate is J_1, and the corresponding angular displacement is θ_1 The moment of inertia of the friction block is J_2, and the corresponding angular displacement θ_2. k and c are the equivalent stiffness and damping of the DMF, respectively. The coefficient of friction is expressed as μ, and the engine output torque is denoted by T, as shown in Fig. 3. For the pressure plate, there following torsional vibration differential equation is given:

$$J_1\ddot{\theta}_1 + c\dot{\theta}_1 + k\theta_1 + 3\,\mathrm{sign}\left(\ddot{\theta}_1\right)\sum_{i=1}^{n} F_i\left(r_b\sin\varphi_i + \mu\left(r + r_b\cos\varphi_i\right)\right) = T \tag{5}$$

where 'sign' is a symbolic function.

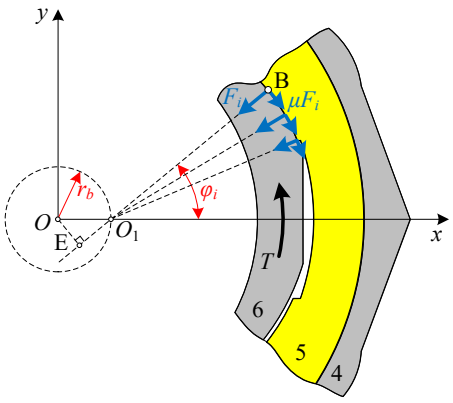

Fig.3. Force analysis of the pressure plate

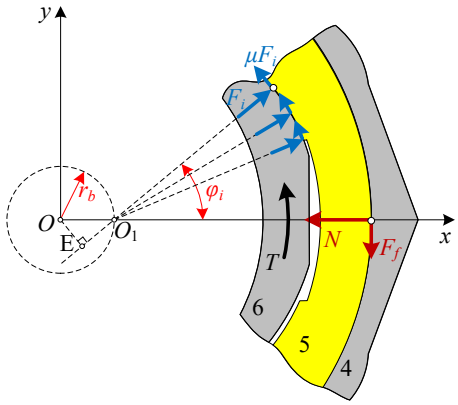

Fig.4. Force analysis of the friction block

As shown in Fig.4, N and F_f are the forces between the friction block and the secondary flywheel in normal and tangential directions, respectively. And the friction block is balanced in the radial direction due to shape constraints. Thus,

$$m_2\dot{\theta}_2^{\,2}l + \sum_{i=1}^{n}\left(F_i\cos\varphi_i - \mu F_i\sin\varphi_i\right) - N = 0 \tag{6}$$

where l is the distance from the friction block center to the point O, and m_2 is the friction block mass.

For the friction block, the following torsional vibration differential equation is given:

$$J_2\ddot{\theta}_2+\operatorname{sign}\left(\dot{\theta}_2\right)\left(\mu NR+M_{fa}\right)-3\operatorname{sign}\left(\ddot{\theta}_1\right)\sum_{i=1}^{n}F_i\left(r_b\sin\varphi_i+\mu\left(r+r_b\cos\varphi_i\right)\right)=0 \quad (7)$$

where M_f is the axial friction torque.

By eliminating the terms containing N and F_i from Equations (5)–(7), the vibration differential equation of the single degree of freedom system is simplified as follows:

$$\begin{aligned}&\left(J_1+3J_2\right)\ddot{\theta}_1+c\dot{\theta}_1+k\theta_1+3\operatorname{sign}\left(\dot{\theta}_1\right)\mu Rm_2\dot{\theta}_1^2l+\\&\operatorname{sgin}\left(\dot{\theta}_1\right)M_f+\frac{\operatorname{sign}\left(\dot{\theta}_1\ddot{\theta}_1\right)\mu RC_2}{C_1}\left(T-J_1\ddot{\theta}_1-c\dot{\theta}_1-k\theta_1\right)=T\end{aligned} \quad (8)$$

where,

$$\begin{cases}C_1=G\sum_{i=1}^{n}\left(\sin\varphi_i\right)^{\frac{10}{9}}\left(r_b\sin\varphi_i+\mu\left(R_1+r_b\cos\varphi_i\right)\right)\\C_2=G\sum_{i=1}^{n}\left(\sin\varphi_i\right)^{\frac{10}{9}}\left(\cos\varphi_i-\mu\sin\varphi_i\right)\\G=\left(\frac{h^{0.8}E^{*0.9}}{1.36}r_b\right)^{\frac{10}{9}}\end{cases} \quad (9)$$

Fig. 5 shows the torque characteristics of the DMF. The equivalent stiffness of the DMF, which consists of two stages, can be expressed as :

$$k=\begin{cases}k_1 & -\beta<\theta_1<\beta\\k_2 & \beta<\theta_1 \text{ or } \theta_1<-\beta\end{cases} \quad (10)$$

where β is the relative angle corresponding to the change in stiffness.

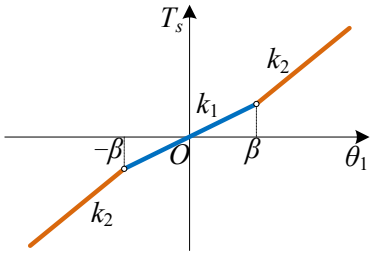

Fig. 5. Torque characteristics of the DMF

The output torque of a engine after it starting is constantly changing for the cyclical change of the engine cylinder pressure and the inertial force generated

by the reciprocating motion of the crank-link mechanism in internal combustion engines. According to Ref [20], the output torque of a engine can be expressed in the following formula:

$$T = T_0 + \sum_{r=1}^{\infty} T_r \sin\left(r\omega t + \psi_r\right) \tag{11}$$

where T_0 is the average torque, r is the number of simple harmonics, T_r is the amplitude of the r-order simple harmonic torque, ψ_r is the corresponding initial phase, ω is the crank angular velocity, and t is time.

Simplify the output torque of a engine to be: $T=T'\sin\omega t$, where T' is a constant. Assume that the differential equation of vibration (8) has the following form of solution: $\theta_1 = A\sin\left(\omega t - \gamma\right) = A\sin\vartheta$, where A is the amplitude and γ is the phase difference. And here let:

$$\begin{aligned} f\left(\theta_1,\dot{\theta}_1,\ddot{\theta}_1\right) &= k\theta_1 + 3\,\mathrm{sign}\left(\dot{\theta}_1\right)\mu R m_2 \dot{\theta}_1^2 l + \mathrm{sign}\left(\dot{\theta}_1\right) M_f \\ &+ \frac{\mathrm{sign}\left(\dot{\theta}_1\ddot{\theta}_1\right)\mu R C_2}{C_1}\left(T - J_1\ddot{\theta}_1 - c\dot{\theta}_1 - k\theta_1\right) \end{aligned} \tag{12}$$

According to the equivalent linearization method [21], only the first harmonic response of the system is considered here, and the higher harmonic response is ignored. $f\left(\theta_1,\dot{\theta}_1,\ddot{\theta}_1\right)$ is expanded using the Fourier transform into the following form:

$$f\left(\theta_1,\dot{\theta}_1,\ddot{\theta}_1\right) = f\left(A,\vartheta\right) = a_0 + a_1\cos\vartheta + a_2\sin\vartheta \tag{13}$$

where,

$$\begin{cases} a_0 = \dfrac{1}{2\pi}\displaystyle\int_0^{2\pi} f\left(A,\vartheta\right)d\vartheta \\ a_1 = \dfrac{1}{\pi}\displaystyle\int_0^{2\pi} f\left(A,\vartheta\right)\cos\vartheta d\vartheta \\ a_2 = \dfrac{1}{\pi}\displaystyle\int_0^{2\pi} f\left(A,\vartheta\right)\sin\vartheta d\vartheta \end{cases} \tag{14}$$

Based on Equations (10), (12), (13) and (14), the following equivalent equation can be obtained by simplifying Equation (8):

$$J_e\ddot{\theta}_1 + c_e\dot{\theta}_1 + k_e\theta_1 = T'\sin\omega t \tag{15}$$

where, $J_e=J_1+3J_2$. k_e and c_e are equivalent stiffness and damping, respectively, which can be calculated as Equations (16) and (17).

(1) When $A<\beta$

$$\begin{cases} k_e = k_1 + \dfrac{2\mu RC_2}{\pi C_1} c\omega \\ c_e = c + \dfrac{8\mu m_2 lR}{\pi} A\omega - \dfrac{2\mu RJ_1 C_2}{\pi C_1}\omega + \dfrac{4M_f}{\pi A\omega} + \dfrac{2\mu RC_2}{\pi C_1 \omega} k_1 \end{cases} \tag{16}$$

(2) When $A \geq \beta$

$$\begin{cases} k_e = k_2 + \dfrac{2\mu RC_2}{\pi C_1} c\omega + \dfrac{2}{\pi}\left(\arcsin\left(\dfrac{\beta}{A}\right) - \dfrac{\beta}{A}\sqrt{1-\left(\dfrac{\beta}{A}\right)^2} \right)\left(k_1 - k_2\right) \\ c_e = c + \dfrac{8\mu m_2 lR}{\pi} A\omega - \dfrac{2\mu RJ_1 C_2}{\pi C_1}\omega + \dfrac{4M_f}{\pi A\omega} + \dfrac{2\mu RC_2}{\pi C_1 \omega}\left(k_2 + \left(k_1 - k_2\right)\left(\dfrac{\beta}{A}\right)^2 \right) \end{cases} \tag{17}$$

The amplitude A, phase γ, and the excitation frequency ω have the following nonlinear relationship:

$$\begin{cases} A = \dfrac{T'}{\sqrt{\left(k_e - J_e\omega^2\right)^2 + \left(c_e\omega\right)^2}} \\ \gamma = \arctan\dfrac{c_e\omega}{k_e - J_e\omega^2} \end{cases} \tag{18}$$

The approximate analytical solution of amplitude A and phase γ can be obtained by solving the system of nonlinear Equations (15), (16), (17), and (18).

5. Result and analysis

The main parameters of the DMF studied in this work are as follows: r=60 mm, R=92.5 mm, J_1=0.15 kg·m^2, J_2=0.17×10^{-3} kg·m^2, m_2=0.083 kg, l=70.9 mm, M_f=5 N·m, μ=0.06, r_b=16 mm, h=10 mm, c=0.1N·m·s/°. The angle φ formed by the contact area between the pressure plate and the friction block in the circumferential direction is 30°~60°. The first stage torsional stiffness of the DMF (the range of the torsional angle is: –16°~16°) is k_1=10 N·m/°, and the second stage stiffness is k_2=30 N·m/°. Table 1 shows the main material properties of the friction block, secondary flywheel, and pressure plate.

Table 1

The material properties

	Secondary flywheel	Friction block	Pressure plate
Material	steel	Pa66	steel
Elastic modulus/GPa	206	8.3	206
Poisson's ratio	0.3	0.28	0.3

The DMF frequency characteristics are obtained through calculation and analysis with the amplitude of the input torque T' was set as 50 N·m, 100 N·m, 150 N·m, and 200 N·m, respectively, as shown in Fig. 6 and 7. When the input torque is small, the torsional angle of the DMF does not exceed 16°. At this time, only the first stage stiffness works, and the frequency characteristics have linear characteristics. Besides, the DMF frequency (amplitude-frequency, phase-frequency) characteristics curves are continuous and smooth changing. The response vibration amplitude increases with the addition of the input torque. When the input torque is large, the torsional angle of DMF will exceed 16°, and the first and second stages stiffness of the DMF act simultaneously. In addition, the system has nonlinear frequency characteristics, the amplitude-frequency characteristic curve curves to the right, and there will be a jump on the frequency (amplitude-frequency, phase-frequency) response curve, which are unstable.

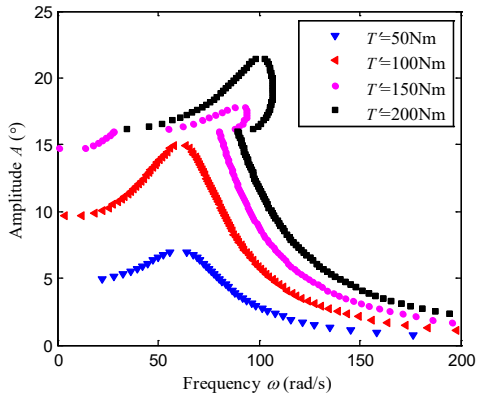

Fig. 6. Amplitude-frequency characteristic

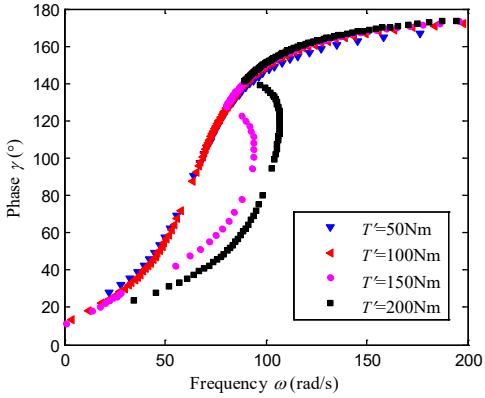

Fig. 7. Phase-frequency characteristic

The equivalent torsional stiffness of the DMF is shown in Fig. 8. It can be concluded that the equivalent stiffness will gradually turn larger when the excitation frequency increases. And when the stiffness of the elastic component is in the variable stage, the equivalent stiffness of DMF will produce a significant jump in the frequency region where the amplitude-frequency characteristics jump. If only the first stage stiffness of the elastic component works, the equivalent stiffness varies with the excitation frequency are basically the same under different torques.

As shown in Fig. 9, the equivalent damping of DMF is large in the low-frequency region, especially when the excitation frequency is below 10 rad/s. At this time, the corresponding speed of the engine is also relatively low, which means that at low speed, such as the engine start condition, the DMF has large equivalent damping. As a result, the impact and torsional vibration in the system can be reduced at this time. With the rise of engine speed, the equivalent damping of DMF will gradually decrease with the increase of the corresponding excitation

frequency, especially since the damping is small under the high-frequency torsional vibration of normal driving. Thus, the power and energy consumption generated by the small damping is reduced. In addition, if the amplitude of the excitation torque becomes larger, the equivalent damping will also increase.

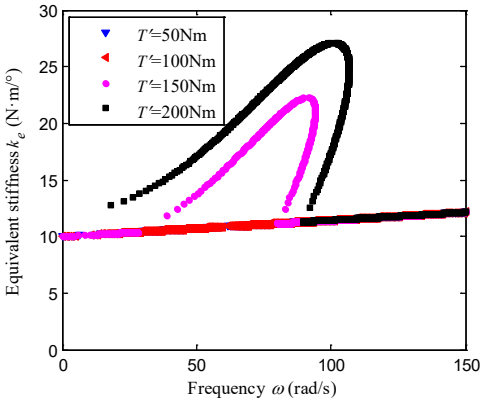

Fig. 8. Equivalent stiffness of DMF

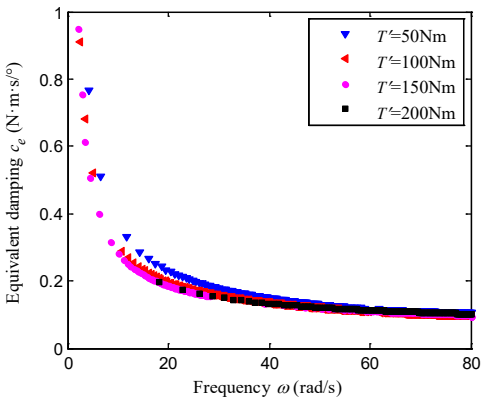

Fig. 9. Equivalent damping of DMF

In order to verify the effectiveness of the theoretical model and approximate solution, the Runge Kutta numerical integration method is used to analyze the forced vibration response of the system. The amplitude of the excitation torque is taken as 200 N·m, and the excitation frequencies are 40 rad/s, 80 rad/s, and 120 rad/s, respectively. According to the torsional vibration differential equation (8) of the system, the time history of the relative angular displacement of the DMF is obtained and compared with the approximate analytical solution (18) of the steady-state forced vibration of the system.

When the excitation frequency is ω=40 rad/s, as shown in Fig. 10, the overall amplitude of θ_1 solved by approximate analytical and numerical methods is 16.3° and 17.8°, respectively. Through the spectrum analysis of the numerical solution, the time history of the numerical solution can be divided into several different frequencies (ω, 3ω, and 5ω). In addition, the frequency of the term that plays a major role is ω. The amplitude at frequency ω is 14.78°. When the excitation frequency ω is at 80 rad/s, the time history and spectrum of θ_1 solved by the approximate analytical and numerical methods are shown in Fig. 11. The amplitude obtained by approximate analytical solution is 18.7°. The time history can also be divided into several different frequencies (ω, 3ω, and 5ω). And the frequency of the main simple harmonic motion term is ω with an amplitude of 18.67°. When the excitation frequency ω is increase to 120 rad/s, the overall amplitude of the time history of θ_1 solved by approximate analytical and numerical methods is 7.3° and 6.5°, respectively, as shown in Fig. 12.

Therefore, the nonlinear approximate analytical solution of the DMF obtained by the equivalent linearization method is similar to the result obtained by the Runge Kutta numerical integration method when the system reaches steady-

state, which shows the effectiveness of the analytical solution for this kind of problems.

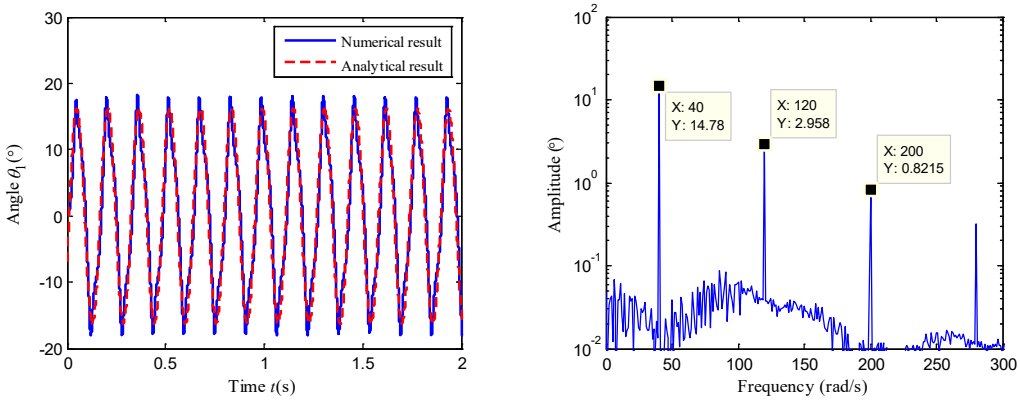

(a) Comparison of the numerical and analytical results (b) Spectrum of the numerical time history

Fig.10. Time history and spectrum of θ_1 when ω=40 rad/s

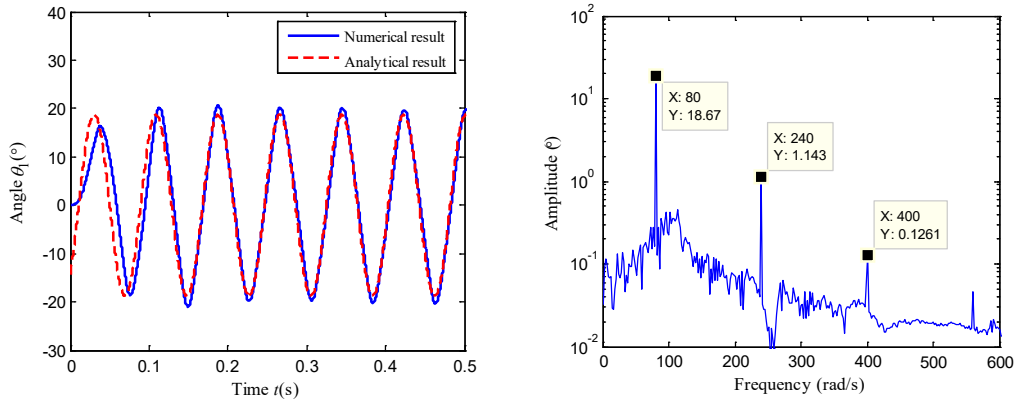

(a) Comparison of the numerical and analytical results (b) Spectrum of the numerical time history

Fig. 11. Time history and spectrum of θ_1 when ω=80 rad/s

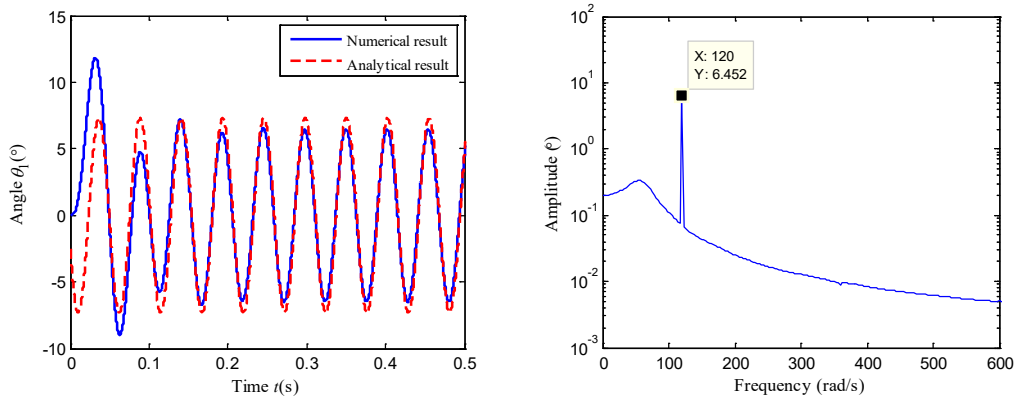

(a) Comparison of the numerical and analytical results (b) Spectrum of the numerical time history

Fig. 12. Time history and spectrum of θ_1 when ω=120 rad/s

6. Conclusions

In this paper, to analyze the vibration characteristics of a dual mass flywheel (DMF) under the influence of variable stiffness and frictional contact in the structure, the dynamic analysis model of the DMF and the corresponding nonlinear torsional vibration differential equation were established. The nonlinear vibration frequency characteristics, equivalent stiffness, and equivalent damping of the DMF at different input torque amplitudes were analyzed by applying equivalent linearization method. By comparing the results of numerical method and equivalent linearization method, the effectiveness of the theoretical model is verified. The following conclusions can be obtained:

(1) The response amplitude of system vibration will become larger with the increase of the input torque. When the input torque is small and only the first-stage stiffness of the DMF works, its frequency characteristics have linear characteristics.

(2) When the input torque of the engine is so large that the first and second stage stiffness of the DMF act simultaneously, the system has nonlinear frequency characteristics, the amplitude-frequency characteristic curve is inclined to the right, and there will be a jump on the frequency response curve.

(3) With the increase of the excitation frequency, the equivalent stiffness gradually becomes larger. When the stiffness of the elastic component is in the change stage, the equivalent stiffness of the DMF will produce an abrupt variation in the frequency region where the amplitude-frequency characteristics jump. If the stiffness of the elastic component does not change, the equivalent stiffness under different torques is basically the same as the excitation frequency changes.

(4) The DMF has large equivalent damping at low speeds, while it will gradually decrease with the increase of the excitation frequency.

Acknowledgements

This work was supported by the National Natural Science Foundation of China (Grant Nos. 51805167 and 52265011), the Natural Science Foundation of Jiangxi Province (Grant No. 20171BAB216029), and the Foundation of Educational Department of Jiangxi Province (Grant No. GJJ170403).

R E F E R E N C E S

[1]. *L. P. Zeng, L. Q. Song, J. D. Zhou,* "Design and elastic contact analysis of a friction bearing with shape constraint for promoting the torque characteristics of a dual mass flywheel," Mechanism and Machine Theory, **vol. 92**, 2015, pp. 356–374.

[2]. *T. S. Kang, S. K. Kauh, K. P. Ha,* "Development of the displacement measuring system for a dual mass flywheel in a vehicle," Proceedings of the Institution of Mechanical Engineers, Part D: Journal of Automobile Engineering, **vol. 223**, no. 10, 2009, pp. 1273–1281.
[3]. *S. Sangue, G. Lepoint, T. Le Bournault,* "New approach to measure instantaneous angular behavior of a dual mass flywheel," Seoul 2000 World Automotive Congress, Seoul, Korea, 2000, pp. 12–15.
[4]. *S. Theodossiades, M. Gnanakumarr, H. Rahnejat, et al.,* "Effect of a dual-mass flywheel on the impact-induced noise in vehicular powertrain systems," Proceedings of the Institution of Mechanical Engineers, Part D: Journal of Automobile Engineering, **vol. 220**, no. 6, 2006, pp. 747–761.
[5]. *X. L. Tang, X. S. Hu, Wei. Yang, et al.,* "Novel torsional vibration modeling and assessment of a power-split hybrid electric vehicle equipped with a dual-Mass flywheel," IEEE Transactions on Vehicular Technology, **vol. 67**, no. 3, 2018, pp. 1990–2000.
[6]. *V. Berbyuk,* "Design optimization of torsional vibration absorbers for heavy-duty truck drivetrain systems," Vibration, **vol. 2**, no. 3 , 2019, pp. 240–264.
[7]. *L. Q. Song, L. P. Zeng, S. P. Zhang, et al.,* "Design and analysis of a dual mass flywheel with continuously variable stiffness based on compensation principle," Mechanism and Machine Theory, **vol. 79**, 2014, pp. 124–140.
[8]. *L. Chen, W. K. Shi, Z. Y. Chen,* "Research on dynamic behavior of torsional absorber in powertrain system considering nonlinear factors," Journal of Vibration and Control, **vol. 27**, no. 13, 2021, pp. 1656–1667.
[9]. *L. P. Zeng, Q. P. Chen, X. X. Yuan, et al.,* "Study on nonlinear vibration of vehicle dual mass flywheels with three-stage piecewise stiffness," China Mechanical Engineering, **vol. 29**, no. 20, 2018, pp. 63–69.
[10]. *L. Q. Song, X. F. Zhao, Z. H. He, et al.,* "Study on analysis model and inherent characteristics of torsional vibration of the dual mass flywheel-circumferential," Journal of Mechanical Engineering, **vol. 45**, no. 11, 2009, pp. 99–105.
[11]. *W. B. Ren, Y. H. Chen, G. F. Zhai, et al.,* "Research on non-linear vibration characteristics of contact system for switching electrical apparatus used in aerospace," Journal of Vibration and Shock, **vol. 26**, no. 12, 2007, pp. 154–156.
[12]. *Y. M. He, A. B. Hao,* "Calculation of gear meshing stiffness and dynamic simulation based on ANSYS workbench," Journal of Shenyang University of Technology, **vol. 42**, no. 2, 2020, pp. 191–196.
[13]. *H. Ahmadian, M. Rajaei,* "Identification of Iwan distribution density function in frictional contacts," Journal of Sound and Vibration, **vol. 333**, no. 15, 2014, pp. 3382–3393.
[14]. *A. Meziane, L. Baillet, B. Laulagnet,* "Experimental and numerical investigation of friction-induced vibration of a beam-on-beam in contact with friction," Applied Acoustics, **vol. 71**, no. 9, 2010, pp. 843–853.
[15]. *Y. L. Wang, X. P. Qin, S. Huang, et al.,* "Design and analysis of a multi-stage torsional stiffness dual mass flywheel based on vibration control," Applied Acoustics, **vol. 104**, 2016, pp. 172–181.
[16]. *W. K. Shi, Y. Long, Y. D. Lu,* "Study on multistage non-linear dual mass flywheel damper," Journal of Vibration and Shock, **vol. 28**, no. 5, 2009, pp. 92–96.
[17]. *L. P. He, C. G. Xia, S. D. Chen, et al.,* "Parametric investigation of dual-mass flywheel based on driveline start-up torsional vibration control," Shock and Vibration, 2019, No. 3171698.
[18]. *K. L. Johnson,* Contact Mechanics, Cambridge, Cambridge University Press, 1985.
[19]. *C. A. Ding, L. Zhang, F. Z. Zhou, et al.,* "Theoretical formula for calculation of line-contact elastic contact deformation," Tribology, **vol. 21**, no. 2, 2001, pp. 135–138.

[20]. *L. Q. Song, H. E. Niu, L. P. Zeng, et al.,* "A Study on the modeling and torsion attenuation for vehicle powertrain system based on unit analysis," Automotive Engineering, **vol. 37**, no. 8, 2015, pp. 866–874.
[21]. *Y. S. Chen,* Nonlinear Vibration, Beijing, Higher Education Press, 2002.